

Experimental studies on behaviour of tubular T-joints reinforced with grouted sleeve

Shouchao Jiang¹, Xiaonong Guo^{*1}, Zhe Xiong², Yufang Cai³ and Shaojun Zhu¹

¹ Department of Building Engineering, Tongji University, Shanghai 200092, China

² School of Civil and Transportation Engineering, Guangdong University of Technology, Guangzhou 510006, China

³ Xuhui Shanghai Land Reserve Co., Ltd., Shanghai 200030, China

(Received May 11, 2016, Revised December 25, 2016, Accepted February 03, 2017)

Abstract. Tubular joints have been widely used in offshore platforms and space structures due to their merits such as easy fabrication, aesthetic appearance and better static strength. For existing tubular joints, a grouted sleeve reinforced method was proposed in this paper. Experimental tests on five tubular T-joints reinforced with the grouted sleeve and two conventional tubular T-joints were conducted to investigate their mechanical behaviour. A constant axial compressive force was applied to the chord end to simulate the compressive state of the chord member during the tests. Then an axial compressive force was applied to the top end of the brace member until the collapse of the joint specimens occurred. The parameters investigated herein were the grout thickness, the sleeve length coefficient and the sleeve construction method. The failure mode, ultimate load, initial stiffness and deformability of these joint specimens were discussed. It was found that: (1) The grouted sleeve could change the failure mode of tubular T-joints. (2) The grouted sleeve was observed to provide strength enhancement up to 154.3%–172.7% for the corresponding un-reinforced joint. (3) The initial stiffness and deformability were also greatly improved by the grouted sleeve. (4) The sleeve length coefficient was a key parameter for the improved effect of the grouted sleeve reinforced method.

Keywords: connections; failure mode; steel-concrete composite

1. Introduction

The construction of tubular joints is straightforward with the brace members welded directly onto the surface of the chord members. Compared with other joint systems, tubular joints have a lot of advantages such as easy fabrication, aesthetic appearance, material saving and better static strength. Therefore, tubular joints are widely used in offshore platforms and space structures. In practical engineering there are many different kinds of tubular joints, including T-joints, Y-joints, K-joints, X-joints, double K-joints, among others.

For the time being, lots of researchers have devoted to the studies on the mechanical behaviour of tubular joints (Chen and Wang 2003, Christitsas *et al.* 2007). Eight failure modes of tubular joints are summarized, including (1) large plastic deformations of the chord members; (2) punching shear failure of the chord members; (3) local buckling of the chord members; (4) crack of welds; (5) global buckling of the brace members; (6) local buckling of the brace members; (7) yield failure of the brace members under axial force; and (8) large plastic deformations of the chord members under secondary bending moment. The load-bearing capacity of tubular joints is closely related to the loading conditions and their dimensions. In general, the strength of tubular joints depends mainly on the chord

thickness, the ratio of brace diameter to chord diameter, the ratio of brace thickness to chord thickness, the ratio of chord diameter to chord thickness, the angle between chord and brace members and the compressive preload applied to the chord members. The achievements on the mechanical behaviour of tubular joints are systematical and developed. Moreover, the design rules for tubular joints are available in the CIEDCT (2008), GB50017 (2003) and Eurocode 3 (2005).

Recently, more and more attention has been attracted to the development of the tubular joint reinforced method. It is indicated that the load-bearing capacity and stiffness of tubular joints could be improved effectively by enhancing the stiffness of joint intersection. The primary tubular joint reinforced methods involve (1) concrete-filled tubular joints (Liu *et al.* 2015); (2) internally ring-stiffened tubular joints (Ahmadi 2016); (3) chord reinforced tubular joints (Yang *et al.* 2012); (4) doubler (collar)-plate reinforced tubular joints (Chen and Chen 2016, Shao 2016); (5) through-wall bolt reinforced tubular joints (Sharaf and Fam 2013, Aguilera and Fam 2013); and (6) FRP-strengthened tubular joints (Lesani *et al.* 2013, 2014, Pantelides *et al.* 2003). To solve the corrosion problem of carbon steel tubular joints, Feng and Young (2011) proposed cold-formed stainless steel tubular joints. Subsequently, they (Feng and Young 2009) carried out an experimental investigation of concrete-filled stainless steel tubular T- and X-joints to study the behaviour and implications for the design of these joints. Cui and Shao (2015) had investigated the residual static strength of cracked concrete-filled circular steel tubular T-joints.

*Corresponding author, Professor,
E-mail: guo-xiao-nong@tongji.edu.cn

Ahmadi (2016) used the FE method to develop a probability distribution model for the stress concentration factor in tubular KT-joints reinforced with internal ring stiffeners. Experimental tests and finite element analyses on chord reinforced tubular joints under axial compressive force were performed by Yang *et al.* (2012). It is indicated that the static strength can be greatly improved by increasing the chord thickness near the intersection. Shao (2016) investigated the collar plate reinforced tubular joints by means of experimental studies and finite element simulations, and indicated that the doubler plate can provide strength enhancement for the corresponding un-reinforced joints. The effectiveness of through-wall bolts for strengthening T-joints was examined by Aguilera and Fam (2013). The experimental results shows that through-wall bolts increase the joint capacity by 13~29%. Pantelides *et al.* (2003) used the glass fiber reinforced polymer (GFRP) for wrapping the tubular joints. It is showed that retrofitted joints with GFRP reinforcement achieve 1.17 to 1.25 times the capacity of un-reinforced joints. Except for the FRP reinforced method, most of the aforementioned reinforced methods are not suitable for existing tubular joints. However, compared with other reinforced methods, the effectiveness of FRP reinforced method is relatively small. Therefore, a grouted sleeve reinforced method for existing tubular joints was proposed in this paper.

For the application and development of the grouted sleeve reinforced method, this paper is aimed to study the behaviour of existing tubular joints reinforced with the grouted sleeve. A detailed description of the grouted sleeve reinforced method was reported firstly. Subsequently, an experimental program on five tubular T-joints reinforced with the grouted sleeve and two conventional tubular T-joints were conducted to examine the effectiveness of the grouted sleeve method. These reinforced joint specimens were different in the grout thickness, the sleeve length coefficient and the sleeve construction method. The failure mode, ultimate load, stiffness and strain distributions of these joint specimens were discussed finally. The pertinent achievements could be used as a basis for the further study.

2. Grouted sleeve reinforced method

For the grouted sleeve reinforced method, existing tubular joints are strengthened by the grout and sleeve around the joint intersection. The sleeve is connected to the tubular joint tightly through the expandable grout. The construction of the grouted sleeve reinforced tubular T-joints could be divided into four steps, as shown in Fig. 1. Firstly, according to the dimensions of existing tubular joints and the grout thickness, lots of half sleeves are manufactured. Then, two half sleeves are positioned around the joint intersection. Two half sleeves are assembled by weld or FRP. In order to plug up the opening between the chord member and the sleeve, the Silica gel is used. Finally, the expandable grout is poured into the gap between the tubular and the sleeve from the opening around the brace member.

The primary merits of the grouted sleeve reinforced method are concluded as follows: (1) This reinforced

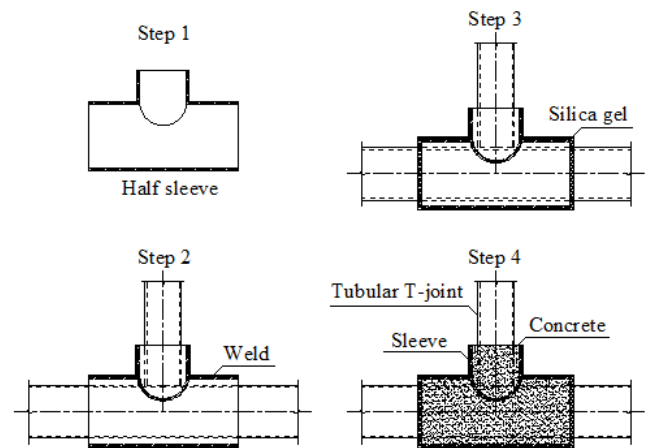


Fig. 1 Tubular T-joint reinforced with the grouted sleeve

method could be used for tubular joints of some existing structures, such as truss structures and reticulated shells; (2) the sleeve could be manufactured in advance, leading to an ease and rapidness of construction of some tubular joints, such as T-, K- and X-joints; (3) The impact property and load-bearing capacity of tubular joints reinforced with the grouted sleeve could be improved greatly. These merits provide a widespread application prospect for tubular joints.

3. Experimental program

In the following section, dimensions and parameters of test specimens, material properties, strain and displacement measurements, test setup and instrumentation and test procedure were described in details.

3.1 Specimens

The compression tests were performed on five tubular T-joints reinforced with the grouted sleeve and two conventional tubular T-joints as reference. All the specimens were fabricated with brace member fully welded to the center of the continuous chord member perpendicularly. These joint specimens were tested under combined brace and chord axial compression loads. The chord load was 180 kN, which represent 15% of the pure axial strength of the chord member. The chord load was kept constant during gradual application of the load on the brace member until the joint specimens were damaged. These joint specimens could be divided into two groups (ZHU group and ZHI group). There were four joint specimens ZHU1~ZHU4 in the ZHU group, while there were three joint specimens ZHI1~ZHI3 in the ZHI group. The main difference of the two groups was the brace thickness t_b of the basic tubular joint. The dimensions of the basic tubular joint and the detailed information of the joint specimens are shown in Fig. 2 and Table 1, respectively. The brace and chord members were fabricated from circular hollow tubes. The cross-section of the chord member was 168 mm × 8 mm, while the cross-section of the brace member was 114 mm × t_b . For the joint specimens in ZHU group, t_b is 6 mm. For the joint specimens in ZHI group, t_b is 4 mm. Joint

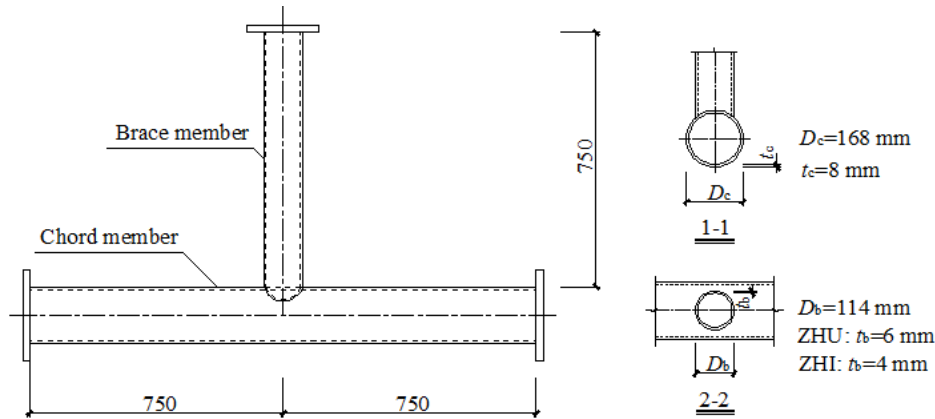


Fig. 2 Dimensions of the basic tubular joint

Table 1 Detailed information of joint specimens

Specimens	Chord (mm)		Brace (mm)			Grout			Sleeve		Construction
	D_c	t_c	Length	D_b	t_b	Length	S_c	t_c (mm)	t_d (mm)	α	
ZHU1	168	8	750	114	6	750					
ZHU2	168	8	750	114	6	750	D14	7	6	1	Weld
ZHU3	168	8	750	114	6	750	D14	19.5	6	1	Weld
ZHU4	168	8	750	114	6	750	D14	7	6	1	FRP
ZHI1	168	8	750	114	4	750					
ZHI2	168	8	750	114	4	750	D14	7	6	1	Weld
ZHI3	168	8	750	114	4	750	D14	7	6	1.5	Weld

specimens ZHU2~ZHU4 and ZHI2~ZHI3 were counterparts of joint specimens ZHU1 and ZHI1, respectively. These joint specimens were retrofitted with the grouted sleeve around the joint intersection. The strength of the grout S_c is D14, representing the strength at 14 days of age. The sleeve thickness was 6 mm. Three key parameters were explored in the tubular joint specimens reinforced with the grouted sleeve. They are the grout thickness, the sleeve length coefficient α and the sleeve construction method.

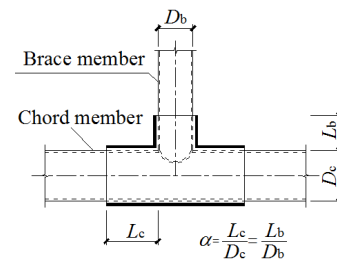


Fig. 3 Length coefficient of the sleeve α

The grout thickness of ZHU3 specimen was 19.5 mm, while the one of the other reinforced specimens was 7 mm. The sleeve length coefficient α was defined as the ratio of overlapping length of the sleeve to the diameter of the corresponding member, as plotted in Fig. 3. The sleeve length coefficient α of ZHI3 specimen was 1.5, while the one of the other reinforced specimens was 1. Weld and carbon fiber reinforced polymer (CFRP) were used for the sleeve construction, as shown in Fig. 4. The sleeve of ZHU4 specimen was assembled by FRP, while the one of the other reinforced specimens was assembled by weld. The joint specimens were shown in Fig. 5.

3.2 Materials

The steel tubes were manufactured from 20# steel (its

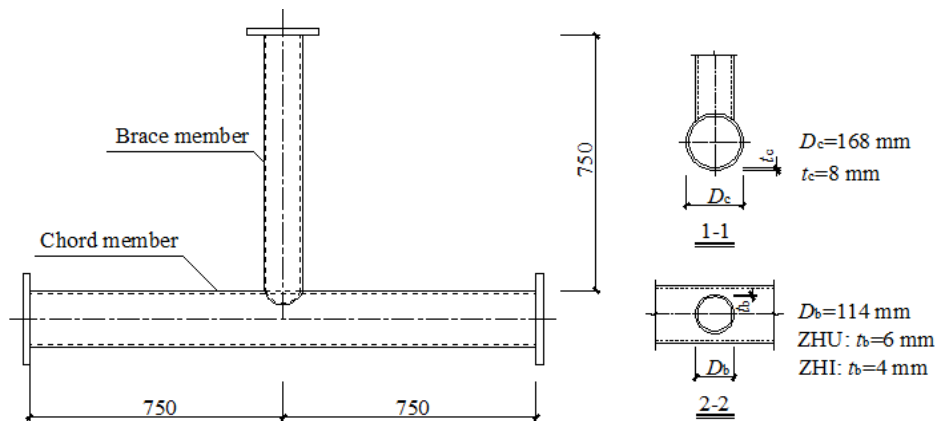


Fig. 2 Dimensions of the basic tubular joint

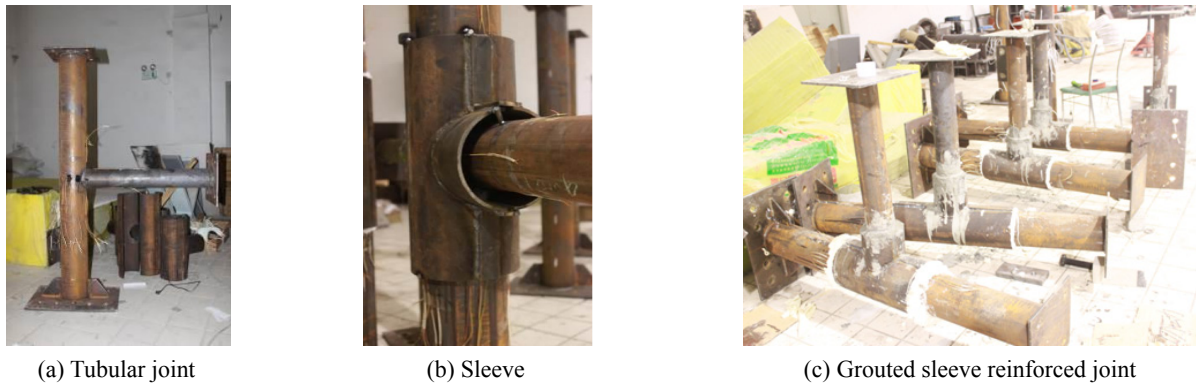


Fig. 5 Joint specimens

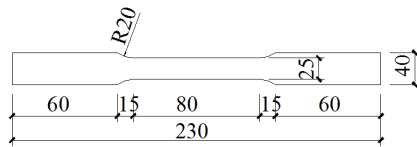


Fig. 6 Plane dimensions of tensile coupons

Table 2 Material properties

Material	No.	Description	E (MPa)	f_y (MPa)	f_u (MPa)	f_{cu} (MPa)
Steel	S-1	For 168 mm × 8 mm chord members	220543	302.18	457.48	
	S-2	For 114 mm × 6 mm brace members	207869	348.43	565.87	
	S-3	For 114 mm × 4 mm brace members	198821	319.64	511.69	
	S-4	For 194 mm × 6 mm of sleeves	204178	308.54	389.05	
	S-5	For 219 mm × 6 mm of sleeves	194386	308.78	466.26	
	S-6	For 140 mm × 6 mm of sleeves	200543	313.38	467.58	
	S-7	For 167 mm × 6 mm of sleeves	208793	356.98	509.38	
	Mean		205109	322.56	481.04	
Grout	C-1	For grout of 19.5 mm thickness	12406			50.31
	C-2	For grout of 7 mm thickness	10528			54.05
	Mean		11467			52.18

nominal yield strength is 275 Mpa and its nominal ultimate strength is 450 Mpa). In order to determine the mechanical properties of the 20# steel, tensile coupon tests were conducted in accordance to the requirements of Chinese Standard of Metallic Materials (GB/T 228-2002). According to the different dimensions of brace members,

chord members and sleeves, seven kinds of tensile coupons were selected. One was cut from the 168 mm × 8 mm chord members; two were cut from the 114 mm × 6 mm and 114 mm × 4 mm brace members; two were cut from the 194 mm × 6 mm and 219 mm × 6 mm chord parts of sleeves and two were cut from the 140 mm × 6 mm and 167 mm × 6 mm brace parts of sleeves. There were three tensile coupons in each kind. Therefore, a total of twenty one tensile coupons were tested. All the tensile coupons have same plane dimensions, as shown in Fig. 6. The mechanical properties of these tensile coupons are listed in Table 2, where E is the elastic modulus, f_y is the yield strength and f_u is the ultimate tensile strength.

To obtain the mechanical properties of the grout, the compressive grout cylinder tests were conducted. The grout cylinders with the dimensions of 40 mm × 40 mm × 160 mm were designed. The grout cylinders were produced by using commercially available materials with normal mixing and curing techniques. The ratio of cement to water to silver sand to bloating agent to water reducing agent is 0.9:0.36:0.35:0.1:0.003. For the grout whose thickness was 7 mm, the level of the water reducing agent was increased. Hence, the grout could be densified during the period of pouring grout. The mechanical properties of the grout are summarized in Table 2, where f_{cu} is the compressive strength.

3.3 Strain and displacement measurements

The measurement plan was comprised of two parts, including arrangement of linear variable differential transducers (LVDTs) and arrangement of strain gauges, as shown in Figs. 7 and 8, respectively.

Seven LVDTs (D1~D7) were adopted to measure the displacement and the deformation of the joint specimens. LVDT D1 was placed under the joint to measure its global vertical displacement. LVDTs D2~D5 were located at the joint intersection vertically to report its deformation. LVDTs D6~D7 were placed at the side face of the chord member horizontally to measure its lateral deformation.

Since the stress at the joint intersection was quite complicate, three-dimensional strain gauges were arranged on the face of the chord member (S1~S11) and the sleeve (S12~S18). Four unidirectional strain gauges (S19~S22) were placed at the side face of the sleeve near its ends in order to measure its longitudinal stress. All the three-

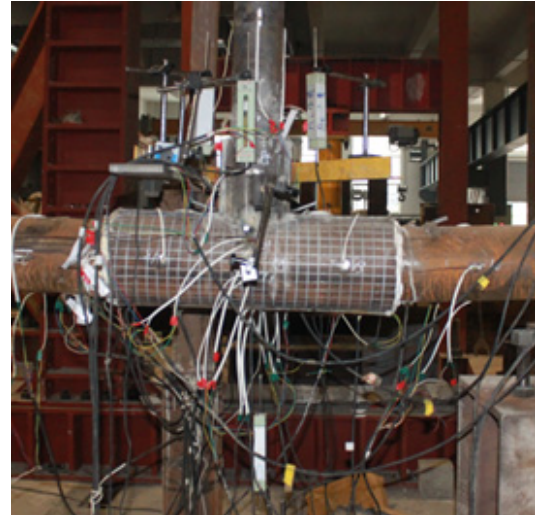
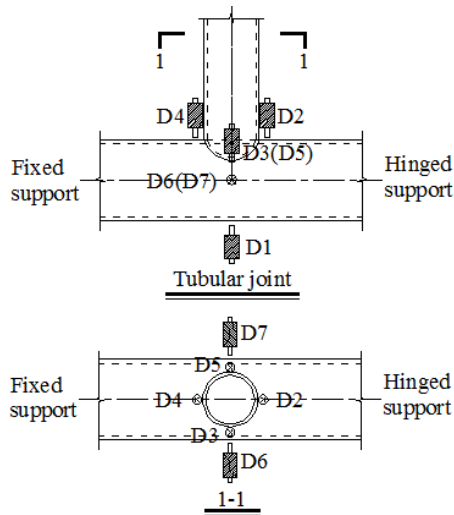


Fig. 7 Arrangement of LVDTs

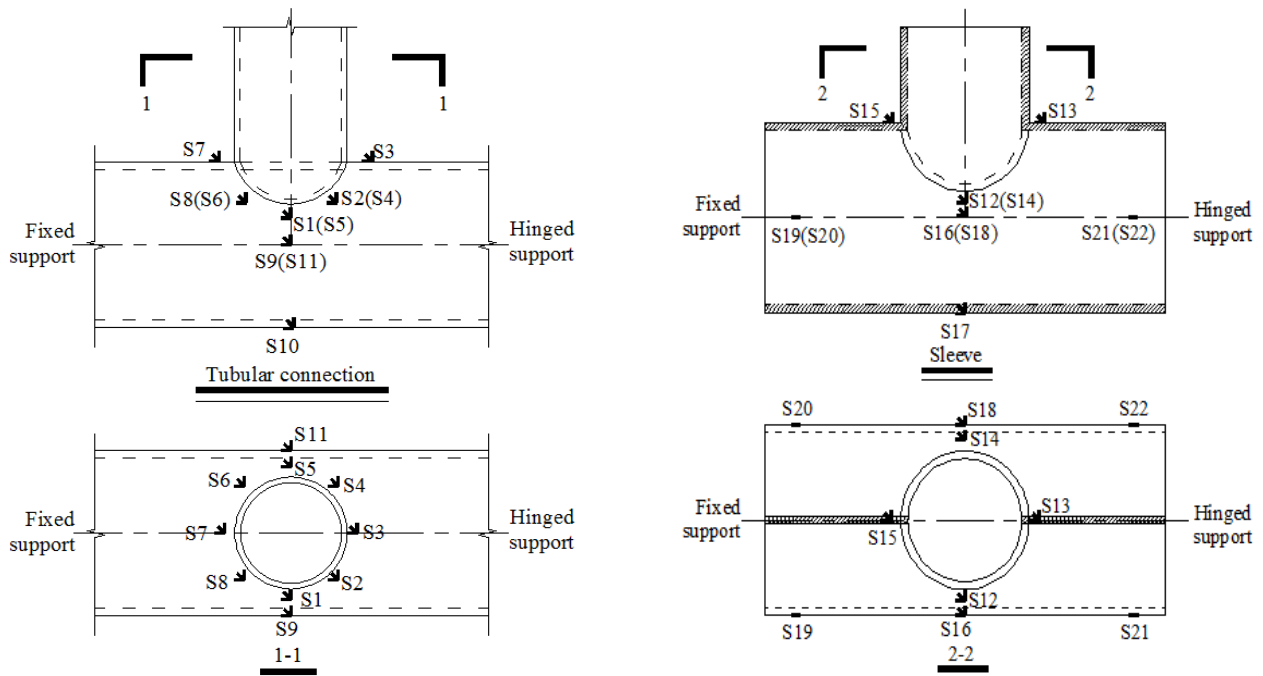


Fig. 8 Arrangement of strain gauges

dimensional strain gauges were arranged 20 mm away from the weld in order to decrease the influence of weld.

3.4 Test rig and procedure

A self-balancing reaction frame was design for the experimental studies on behaviour of tubular T-joints reinforced with the grouted sleeve. All the joint specimens were installed in the same test setup, as shown in Fig. 9. One end of the chord member was fixed to the reaction frame. The other end of the chord member was the rolling support. The close view of the chord end connections was shown in Fig. 10. The axial compression load in the chord member was applied through a horizontal hydraulic jack positioned longitudinally at the rolling end of the chord

member. The vertical hydraulic jack was used to apply the axial compression to the brace member. To eliminate the constraint action of the brace member, a loading ball-plate which was positioned concentrically between the vertical hydraulic jack and the brace member was designed.

During the experimental tests, a preload process was performed firstly to check all test equipment. As everything was examined, the tests were started. Initially, a 180 kN axial compression load was applied to the chord member. This axial compression load was kept in the chord until the end of the test. Subsequently, the brace member was concentrically loaded to failure. At the beginning of the loading process, the tests were performed under force control. The force increment was 20 kN. When the deformation of the joint specimens increased rapidly, the

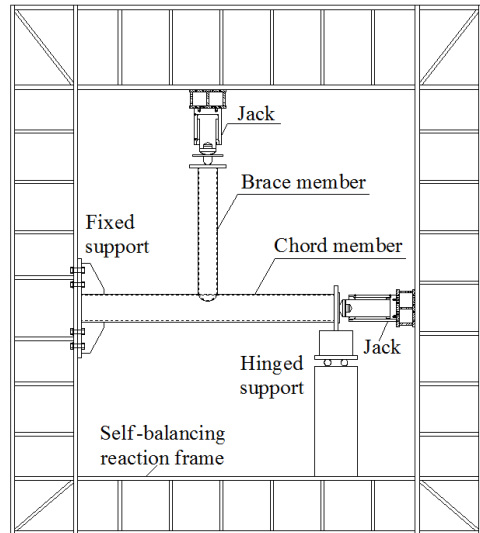


Fig. 9 Test setup of tubular joints

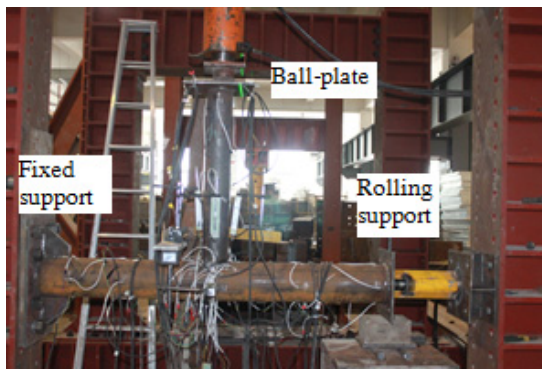


Fig. 10 Connections of member ends

behaviour of the joint specimens entered into non-linear region. At that time, the force control was changed to displacement control until the failure of the joint specimens occurred. The displacement increment was 4 mm. To obtain the complete response of the joint specimens, each load increment lasted for at least 5 minutes.

4. Experimental phenomena and failure modes

The failure modes of the joint specimens are shown in Fig. 11.

For the un-reinforced tubular joint specimens ZHU1 and ZHI1, when the load reached the 85% of the joint ultimate load, visible concave deformation and convex deformation occurred at the top face and the side face of the chord member, respectively. When the load reached the joint ultimate load, the joint deformation developed rapidly, as shown in Figs. 9(a)~(b). Meanwhile, the compression loads of both the chord member and the brace member were declined. Large area of the joint intersection entered into the plastic phase, obviously. Therefore, the failure of the un-reinforced tubular joint specimens ZHU1 and ZHI1 belonged to the ductile failure.

For the reinforced tubular joint specimens ZHU2, ZHI2

and ZHU4, before the load reached the 95% of the joint ultimate load, the joint deformation was small. When the load reached the joint ultimate load, visible deformation occurred at the chord member near the sleeve ends. At the same time, the compression load of the chord member was decreased. At last, the joint specimens ZHU2 and ZHI2 failed with weld cracking and the joint specimen ZHU4 failed with the FRP cracking, as shown in Figs. 9(c)~(e). Thereby, the failure of the reinforced tubular joint specimens ZHU2, ZHI2 and ZHU4 belonged to the brittle failure. Compared with the un-reinforced tubular joint specimens ZHU1 and ZHI1, it could be found that the grouted sleeve could improve the joint stiffness and change the failure mode.

For the reinforced tubular joint specimen ZHU3 whose grout thickness was 19.5 mm, before the load reached the 90% of the joint ultimate load, the joint deformation was small. When the load was close to the joint ultimate load, visible deformation occurred at the chord member near the sleeve ends. Finally, the joint specimen failed with the large plastic deformation of the chord member near the sleeve ends, as shown in Fig. 9(f). Compared with the joint specimen ZHU2, it is observed that the grout thickness could change the failure mode. The joint stiffness improved with the increase of the grout thickness.

For the reinforced tubular joint specimen ZHI3 whose length coefficient of the sleeve was 1.5, before the load reached the 90% of the joint ultimate load, the joint deformation was small. When the load was close to the joint ultimate load, concave deformation and convex deformation occurred at the top face and the side face of the sleeve, respectively. Finally, the joint specimen failed with the large plastic deformation of the chord member and the sleeve. Hence, the failure of the joint specimen ZHI3 belonged to ductile failure. The sleeve length coefficient could also change the failure mode.

Consequently, it is concluded that the grouted sleeve could enhance the joint stiffness and change the failure mode. It is effective methods to avoid the brittle failure of tubular joints reinforced with the grouted sleeve by

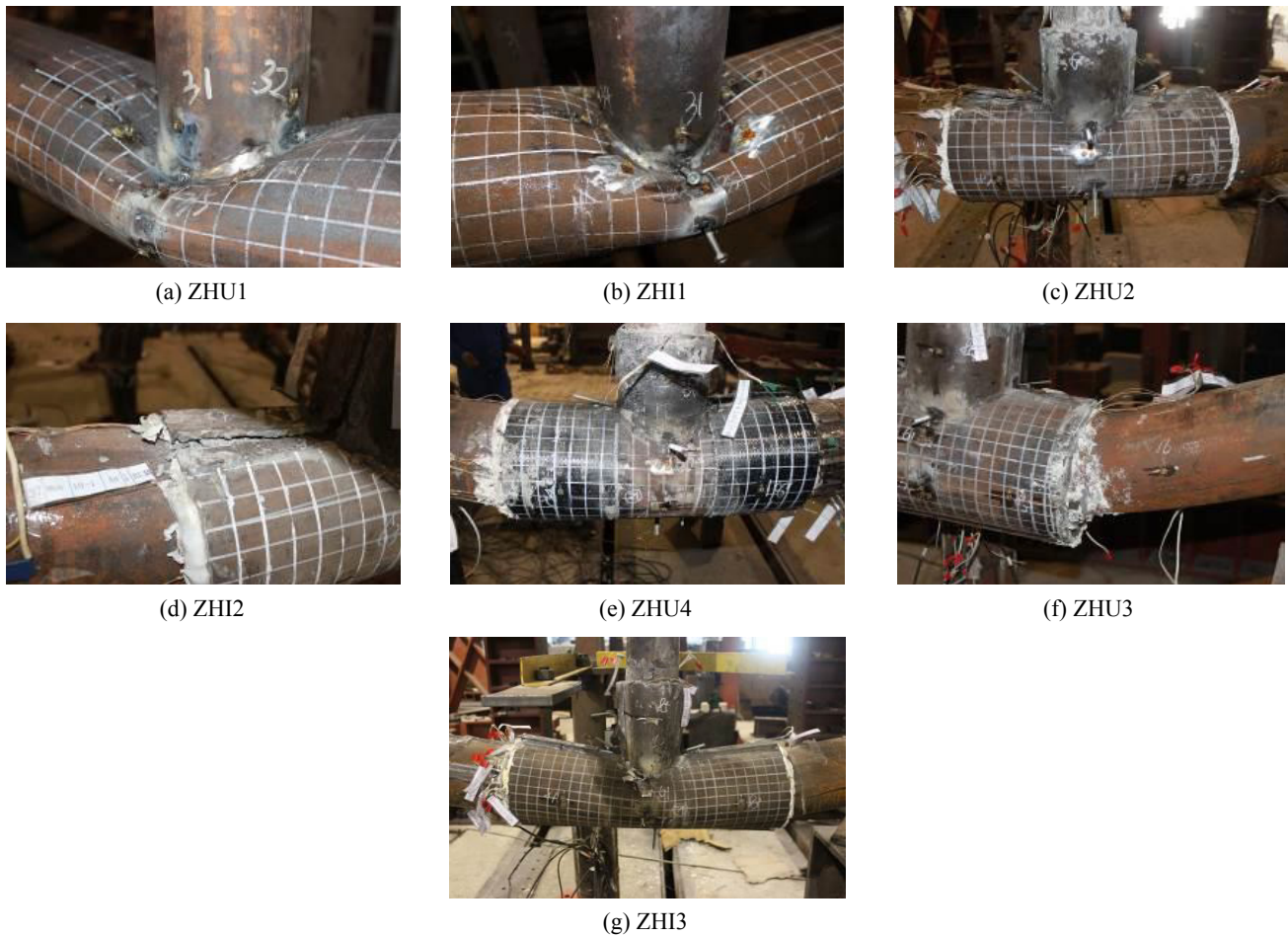


Fig. 11 Failure modes

increasing the grout thickness and the sleeve length coefficient.

Table 3 Initial stiffness and deformability

No.	K_i (kN/mm)	P_u (kN)	d_1 (mm)	No.	K_i (kN/mm)	P_u (kN)	d_1 (mm)
ZHU1	56.6	272.5	19.3	ZHI1	55.1	289.3	19.7
ZHU2	65.5	456.8	54.7	ZHI2	64.2	446.3	44.7
ZHU3	60.3	467.6	66.5	ZHI3	76.3	499.6	41.1
ZHU4	66.2	450.4	61.9				

5. Experimental results

5.1 Load-displacement curves

Fig. 12 shows the load-displacement responses of all the joint specimens based on the global vertical displacement. Their global vertical displacement was recorded by LVDT D1. The initial stiffness of these load-displacement curves K_i and the joint global vertical displacement d_1 at the ultimate load level were summarized in Table 3. Generally, the load ascended almost linearly initially, followed by a non-linear behaviour. When a peak load was reached, a descending response could be observed. According to the

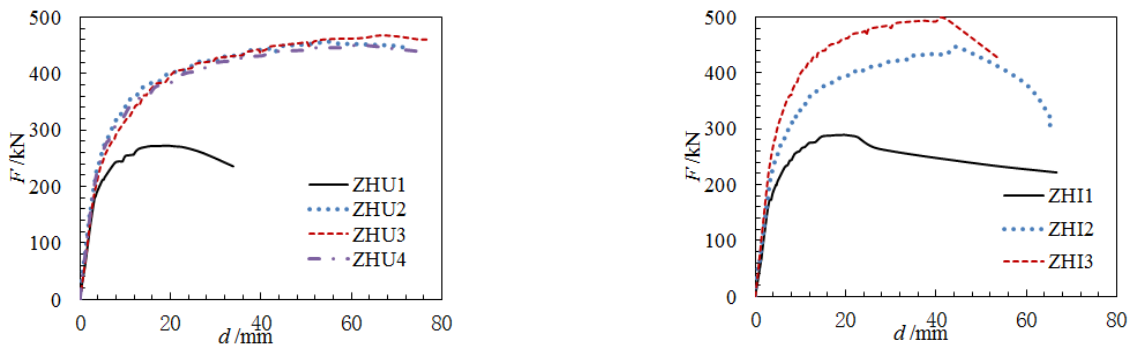


Fig. 12 Load-displacement curves

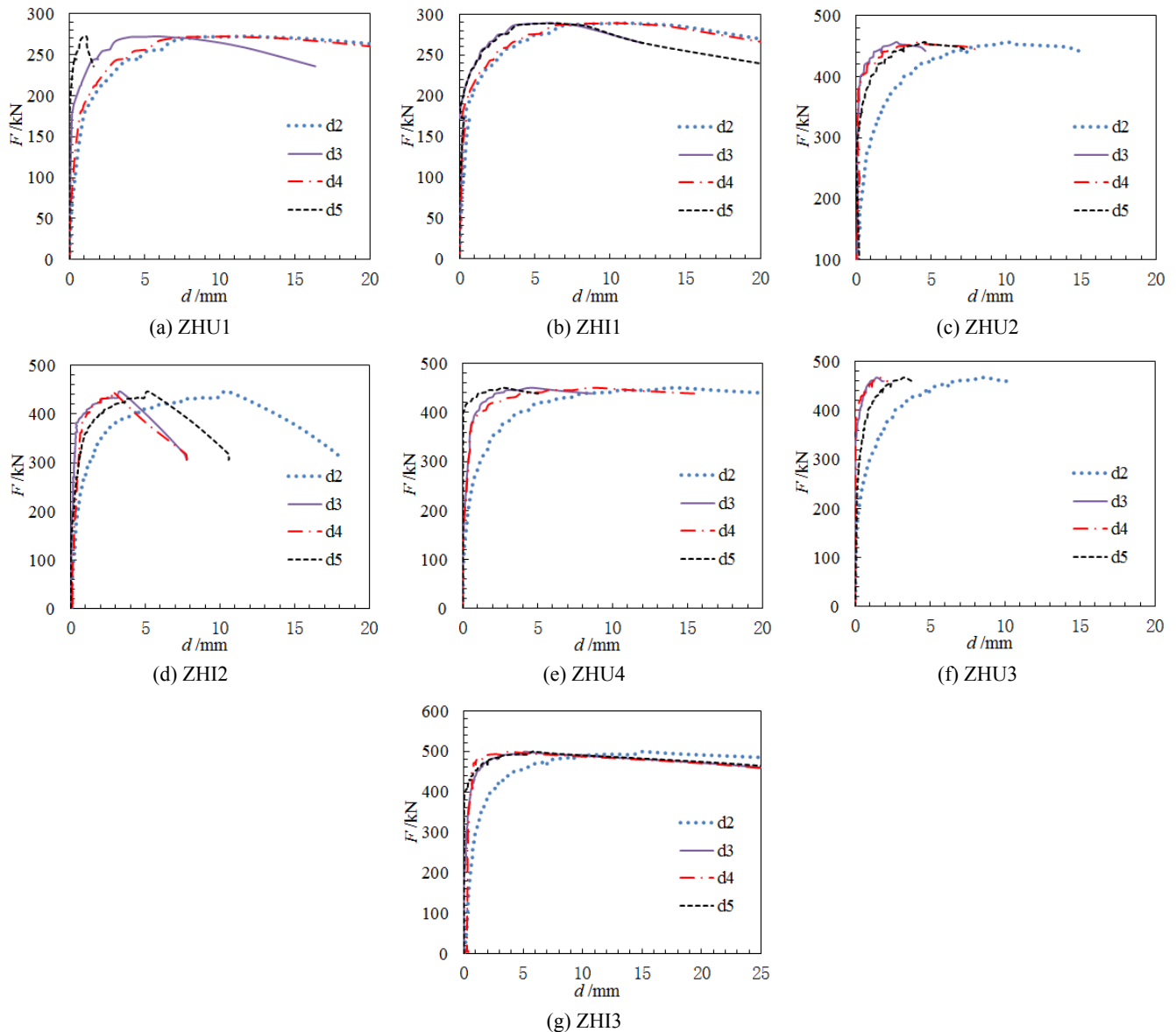


Fig. 13 Load-deformation curves

comparison of these load-displacement curves, it could be found that:

- (1) The grouted sleeve could improve the joint stiffness significantly. Compared with the conventional tubular joint specimens, the stiffness of the joint specimens reinforced with the grouted sleeve was improved by 6.6%~38.4%.
- (2) The joint deformability was also improved by the grouted sleeve. Compared with the conventional tubular joint specimens, the global vertical displacement of the grouted sleeve reinforced joint specimens at the ultimate load level was increased by 180.6%~244.6%.
- (3) The improved effect of the weld sleeve on the behaviour of tubular joints was very close to the one of the FRP sleeve.
- (4) The joint stiffness developed with the increase of the sleeve length coefficient. For the joint specimens

ZHI2 and ZHI3, the sleeve length coefficient was increased from 1 to 1.5, leading to 18.9% improvement of the joint initial stiffness.

The load-deformation curves of the joint intersection are plotted in Fig. 13. The joint deformation $d_2 \sim d_5$ was obtained by the displacement D2~D5 minus the displacement D1. The joint deformation $d_2 \sim d_5$ at the ultimate load level was listed in Table 4. It is observed that:

- (1) The symmetrical deformation d_3 and d_5 agreed well with each other initially, indicating that the compression load was applied to the brace member axially. Subsequently, due to the generation of the secondary bending moment, the symmetrical deformation d_3 and d_5 separated. For the conventional tubular joint specimens, the symmetrical deformation d_2 and d_4 agreed well with each other at the whole test response. However, for

the grouted sleeve reinforced joint specimens, the symmetrical deformation d_2 and d_4 separated with the increase of the compression load. The main reason might be that the stiffness of the joint intersection of the grouted sleeve reinforced joint specimens is very large, due to the different supports of the chord ends, an obvious rotation of the joint specimens occurred.

- (2) The average deformation of d_2 and d_4 was larger than the one of d_3 and d_5 , implying that the local stiffness of D2 and D4 area was smaller than the one of D3 and D5 area on the chord member.
- (3) The grouted sleeve improved the chord stiffness at the joint intersection. Therefore, the average deformation of d_2 and d_4 of the grouted sleeve reinforced joint specimens was smaller than the one

Table 4 Deformation $d_2 \sim d_5$ of tubular connections

No.	d_2 (mm)	d_3 (mm)	d_4 (mm)	d_5 (mm)
ZHU1	11.89	5.83	10.62	1.11
ZHU2	10.11	2.70	4.22	4.57
ZHU3	8.43	1.42	1.71	3.22
ZHU4	14.15	4.58	8.76	2.75
ZHI1	11.24	5.90	10.42	6.39
ZHI2	10.53	3.33	2.81	5.20
ZHI3	14.96	5.14	3.74	5.81

of the unreinforced joint specimens.

The load-lateral deformation curves for the side face of the chord member are shown in Fig. 14. It is shown that the

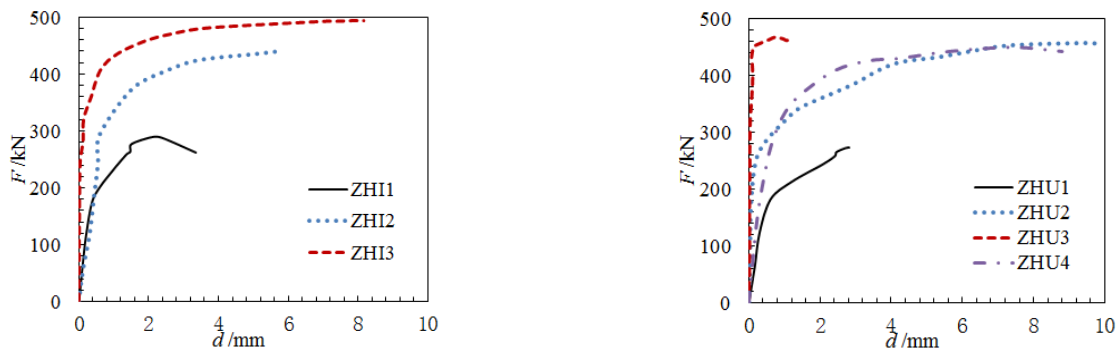


Fig. 14 Load-lateral deformation curves

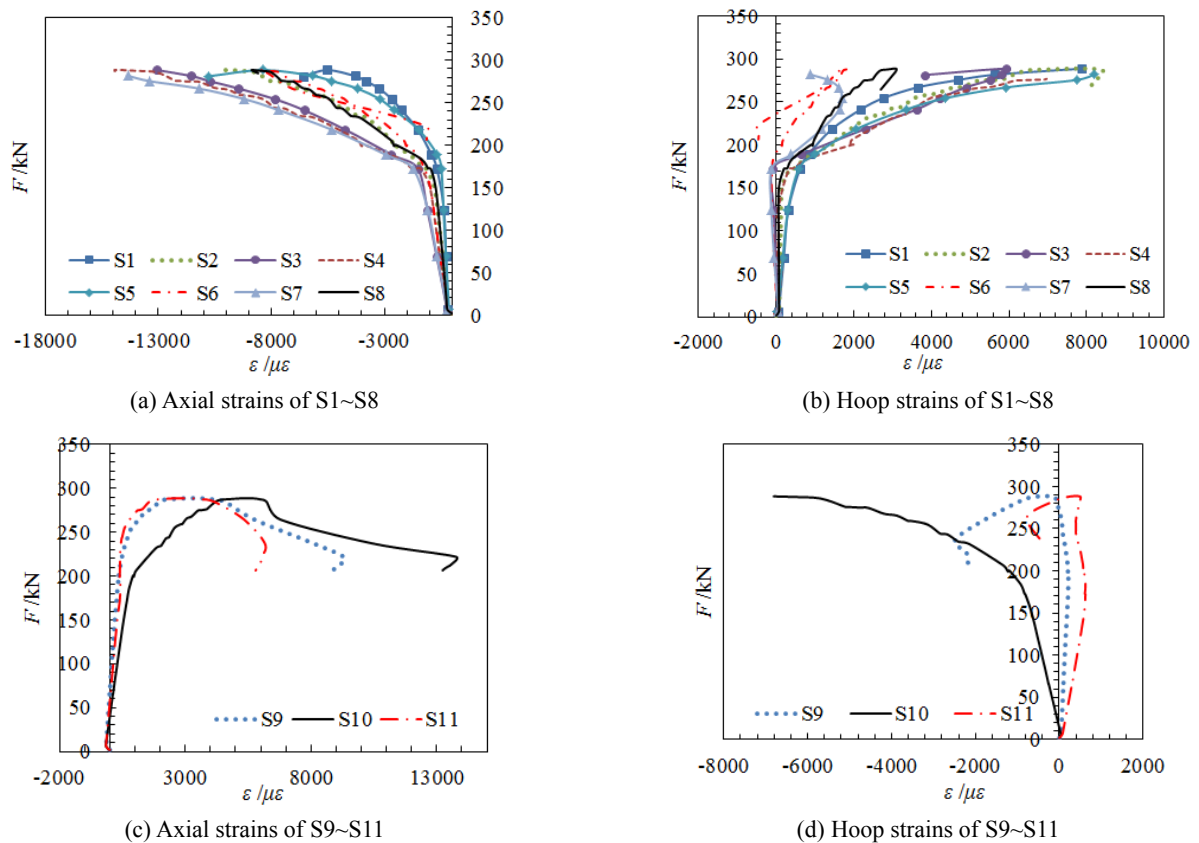


Fig. 15 Load-strain curves of un-reinforced joint specimen ZHI1

grouted sleeve could improve the out-of-plane stiffness of the side face of the chord member.

5.2 Load-strain curves

To explore the stress distributions of the joint specimens, their strains were recorded. The load-strain curves of the un-reinforced joint specimen ZHI1 are shown in Fig. 15.

Fig. 15(a) exhibits the axial strains of S1~S8. The axial strains of S1~S8 performed compressive behaviour. And the axial strains of S3 and S7 were larger than that of S1 and S5 all the time, meaning that the area of S3 and S7 would yield earlier than that of S1 and S5.

Fig. 15(b) shows the hoop strains of S1~S8. At the beginning of the loading process, the hoop strains of S3 and S7 performed compressive behaviour, while the hoop strains of S1 and S5 performed tensile behaviour. Subsequently, when the load was larger than 170 kN, the hoop strains of S3 and S7 turned into the tensile phase. At

the same time, the tensile strains of S1 and S5 developed rapidly. These phenomena signified the buckling of the top face of the chord member at the joint intersection.

Fig. 15(c) plots the axial strains of S9~S11. The axial strains of S9~S11 performed tensile behaviour. And the axial strains of S10 were larger than that of S9 and S11 all the time. The main reason was due to the generation of the bending moment.

Fig. 15(d) shows the hoop strains of S9~S11. Initially, the hoop strains of S10 revealed compressive response, while the hoop strain of S9 and S11 revealed tensile response. When the load was larger than 170 kN, the local stiffness on the chord face at the joint intersection began to decrease. As a result, the hoop strains of S10 increased and the hoop strains of S9 and S11 decreased.

The load-strain curves of the sleeve of the reinforced joint specimen ZHI3 are shown in Fig. 16. The stress distributions of the sleeve were similar to the one of the tubular joint at the joint intersection. For the axial strains, S12~S15 exhibited the compressive behaviour, while

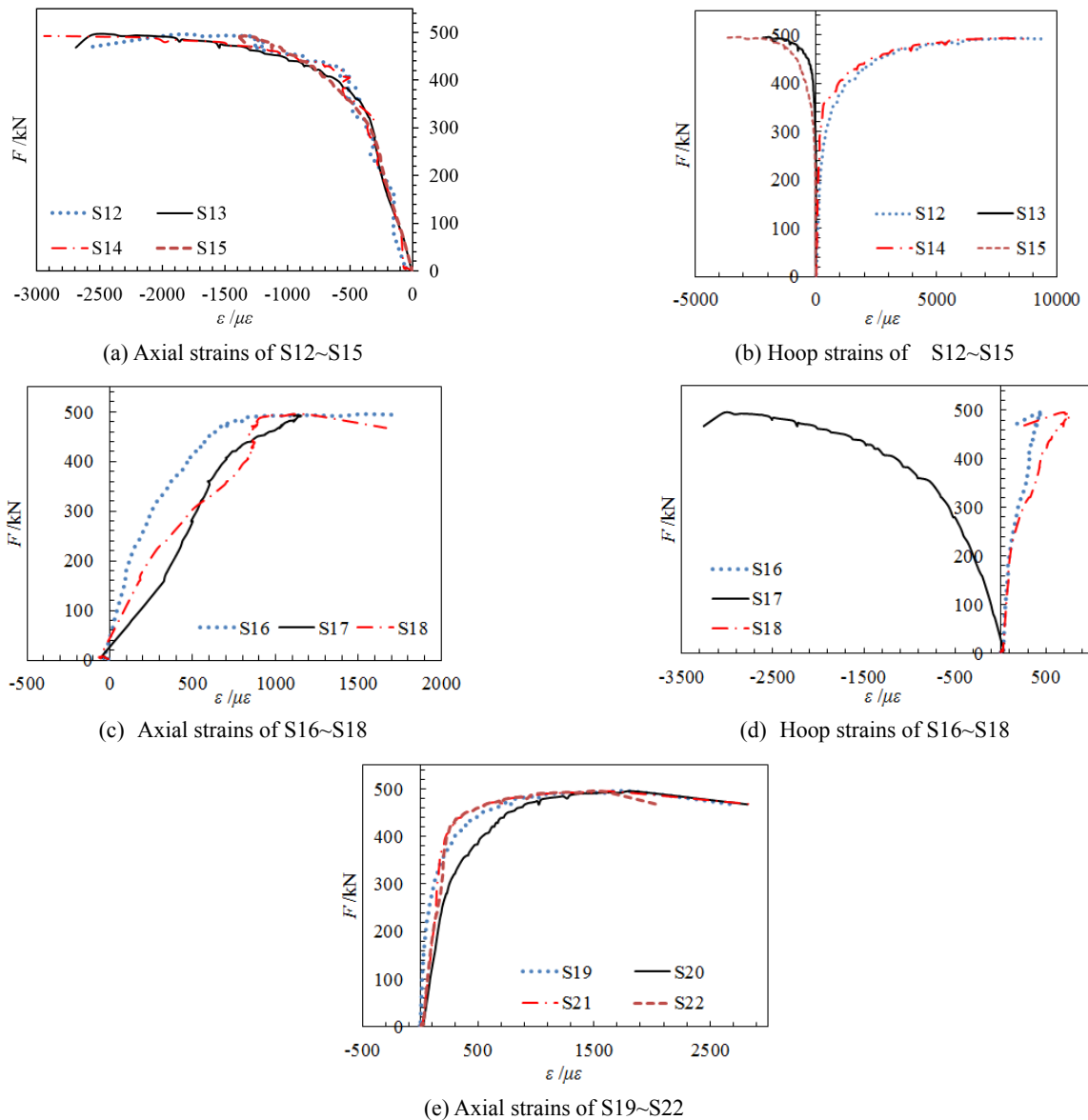


Fig. 16 Load-strain curves of the sleeve of the reinforced joint specimen ZHI2

S16~S22 exhibited the tensile behaviour. For the hoop strains, S13, S15 and S17 exhibited the compressive behaviour, while S12, S14, S16 and S18 exhibited the tensile behaviour.

5.3 Ultimate loads

The existing design rules for the tubular T-joints are available in the CIEDCT (2008), GB50017 (2003) and Eurocode3 (2005). The design equations for the ultimate loads of tubular T-joints are expressed as follows:

In CIEDCT (2008), the design load of the brace member under the criterion of chord plastification is given by Eqs.(1)~(7). N_i^* is the design load of tubular T-joints; n is the normal stress ratio considering the stress of the chord member; N_0 is the axial force of the chord member; $N_{pl,0}$ is the yield axial force of the chord member; M_0 is the chord moment; $M_{pl,0}$ is the ultimate bending moment of the chord; β is the ratio of the brace diameter to the chord diameter; γ is the ratio of the chord radius to the chord thickness.

$$N_i^* = Q_u Q_f \frac{f_{y0} t_0^2}{\sin \theta} \quad (1)$$

$$Q_u = 2.6(1 + 6.8\beta^2)\gamma^{0.2} \quad (2)$$

$$Q_f = (1 - |n|)^{C_1} \quad (3)$$

$$n = \frac{N_0}{N_{pl,0}} + \frac{M_0}{M_{pl,0}} \quad (4)$$

$$N_{pl,0} = A_0 f_{y0} \quad (5)$$

$$M_{pl,0} = W_{pl,0} f_{y0} \quad (6)$$

$$C_1 = 0.45 - 0.25\beta \quad (7)$$

The design equations introduced in GB50017 (2003) are expressed in Eqs. (8)~(10). N_{ct}^{pi} is the design load of tubular T-joints; θ is the angle between the brace member and the chord member; d is the chord diameter; t is the chord thickness; Ψ_n is influence factor on the axial force of the chord member; Ψ_d is size factor; f is the strength of the chord member; σ is the minimum stress generated by the axial compressive force of the chord member; f_y is the yield strength of the chord member; β is the ratio of the brace diameter to the chord diameter.

$$N_{ct}^{pi} = \frac{11.51}{\sin \theta} \left(\frac{d}{t}\right)^{0.2} \Psi_n \Psi_d t^2 f \quad (8)$$

$$\Psi_n = 1 - 0.3 \frac{\sigma}{f_y} - 0.3 \left(\frac{\sigma}{f_y}\right)^2 \quad (9)$$

$$\begin{cases} \Psi_d = 0.069 + 0.93\beta & \beta \leq 0.7 \\ \Psi_d = 2\beta - 0.68 & \beta > 0.7 \end{cases} \quad (10)$$

Table 5 Ultimate loads

No.	Test (kN)	CIEDCT (kN)	GB50017 (kN)	EC3 (kN)
ZHU1	272.5	275.1	271.7	274.1
ZHI1	289.3	275.1	271.7	274.1

In brace member connections subject only to axial forces, considering chord face failure, the design internal axial force $N_{i,Rd}$ adopted in Eurocode 3 Part 1-8 (2005) are expressed in Eqs. (11)~(14). γ is the ratio of the chord radius to the chord thickness; $\sigma_{p,Ed}$ is the value of $\sigma_{0,Ed}$ excluding the stress due to the components parallel to the chord axis of the axial forces in the braces at that joint; β is the ratio of the brace diameter to the chord diameter; $\gamma_{M5} = 1$, is the safety factor of the joint resistance of hollow section structure.

$$N_{i,Rd} = \frac{\gamma^{0.2} k_p f_{y0} t_0^2}{\sin \theta} (2.8 + 14.2\beta^2) / \gamma_{M5} \quad (11)$$

$$\gamma = \frac{d_0}{2t_0} \quad (12)$$

$$k_p = \min \{1 - 0.3n_p (1 + n_p), 1.0\} \quad (13)$$

$$n_p = \frac{\sigma_{p,Ed}}{f_{y0} \gamma_{M5}} \quad (14)$$

Table 5 shows the ultimate loads obtained from the test, CIEDCT (2008), GB50017 (2003) and Eurocode3 (2005). According to Tables 3 and 5, it is found that:

- (1) For the un-reinforced tubular joints, the ultimate loads obtained from the test were very close to that obtained from CIEDCT (2008), GB50017 (2003) and Eurocode3 (2005), verifying the reliability of the test results.
- (2) The grouted sleeve improved the joint strength significantly. Compared with the un-reinforced tubular joints, the ultimate load of reinforced tubular joints was improved by 54.3%~72.7%.
- (3) The improved effect of the weld sleeve on the ultimate load of tubular joints was very close to the one of the FRP sleeve.
- (4) The ultimate load developed with the increase of the sleeve length coefficient. For the joint specimens ZHI2 and ZHI3, the sleeve length coefficient was increased from 1 to 1.5, leading to 11.9% improvement of the ultimate load.

6. Conclusions

The behaviour of tubular T-joints reinforced with the grouted sleeve was investigated. A series of un-reinforced and the grouted sleeve reinforced T-joints was tested. The main conclusions were summarized as follows:

- (1) The main failure mode of the un-reinforced joint specimens was the large plastic deformations of the chord members which belonged to the ductile failure. The main failure modes of the grouted sleeve reinforced joint specimens included the weld cracking, the FRP cracking, the large plastic deformation of the chord member near the sleeve ends and the large plastic deformation of the chord member and the sleeve. Therefore, the grouted sleeve could change the failure mode of tubular T-joints.
- (2) The grouted sleeve could improve the initial stiffness, deformability and ultimate load of tubular T-joints significantly. Compared with the un-reinforced joint specimens, initial stiffness, deformability and ultimate load of reinforced tubular joints were improved by 6.6%~38.4%, 180.6%~244.6% and 54.3%~72.7%, respectively.
- (3) The improved effect of the weld sleeve on the behaviour of tubular joints was very close to the one of the FRP sleeve.
- (4) The sleeve length coefficient was a key parameter for the improved effect of the grouted sleeve. For the joint specimens ZHI2 and ZHI3, the sleeve length coefficient was increased from 1 to 1.5, leading to 11.9% improvement of the ultimate load and 18.9% improvement of the joint initial stiffness.

Acknowledgments

The authors gratefully acknowledge the financial support provided by the Ministry of Science and Technology of China, Grant No. SLDRCE15-B-04.

References

- Aguilera, J. and Fam, A. (2013), "Retrofitting tubular steel T-joints subjected to axial compression in chord and brace members using bonded FRP plates or through-wall steel bolts", *Eng. Struct.*, **48**, 602-610.
- Ahmadi, P. (2016), "A probability distribution model for SCFs in internally ring-stiffened tubular KT-joints of offshore structures subjected to out-of-plane bending loads", *Ocean Eng.*, **116**, 184-199.
- Chen, Y. and Chen, D.F. (2016), "Ultimate capacities formulae of collar and doubler plates reinforced SHS X-joints under in-plane bending", *Thin-Wall. Struct.*, **99**, 21-34.
- Chen, Y.Y. and Wang, W. (2003), "Flexural behavior and resistance of uni-planar KK and X tubular joints", *Steel Compos. Struct., Int. J.*, **3**(2), 123-140.
- Christitsas, A.D., Pachoumis, D.T., Kalfas, C.N. and Galoussis, E.G. (2007), "FEM analysis of conventional and square bird-beak SHS joint subject to in-plane bending moment—experimental study", *J. Constr. Steel Res.*, **63**(10), 1361-1372.
- CIDECT (2008), Design guide for circular hollow section (CHS) joints under predominantly static loading; Cologne, Germany.
- Cui, M.J. and Shao, Y.B. (2015), "Residual static strength of cracked concrete-filled circular steel tubular (CFCST) T-joint", *Steel Compos. Struct., Int. J.*, **18**(4), 1045-1062.
- Eurocode 3 (2005), Design of steel structures—Part 1-8: Design of joints; European Committee for Standardization, EN1993-1-8, CEN, Brussels, Belgium.
- Feng, R. and Young, B. (2009), "Behaviour of concrete-filled stainless steel tubular X-joints subjected to compression", *Thin-Wall. Struct.*, **47**(4), 365-374.
- Feng, R. and Young, B. (2011), "Design of cold-formed stainless steel tubular T- and X-joints", *J. Constr. Steel Res.*, **67**(3), 421-436.
- GB 50017-2003 (2003), Code for design of steel structures; Ministry of housing and urban-rural development of the people's republic of China, General administration of quality supervision, inspection and quarantine of the people's republic of China. [In Chinese]
- GB/T 228-2002 (2002), Metallic materials-tensile testing at ambient temperature; General administration of quality supervision, inspection and quarantine of the People's Republic of China. [In Chinese]
- Lesani, M., Bahaari, M.R. and Shokrieh, M.M. (2013), "Numerical investigation of FRP-strengthened tubular T-joints under axial compressive loads", *Compos. Struct. J.*, **100**, 71-78.
- Lesani, M., Bahaari, M.R. and Shokrieh, M.M. (2014), "Experimental investigation of FRP-strengthened tubular T-joints under axial compressive loads", *Constr. Build. Mater.*, **53**, 243-252.
- Liu, H., Shao, Y., Lu, N. and Wang, Q. (2015), "Hysteresis of concrete-filled circular tubular (CFCT) T-joints under axial load", *Steel Compos. Struct., Int. J.*, **18**(3), 739-756.
- Pantelides, C.P., Nadauld, J. and Cercone, L. (2003), "Repair of cracked aluminum overhead sign structures with glass fiber reinforced polymer composites", *J. Compos. Constr.*, **7**(2), 118-126.
- Shao, Y.B. (2016), "Static strength of collar-plate reinforced tubular T-joints under axial loading", *Steel Compos. Struct., Int. J.*, **21**(2), 323-342.
- Sharaf, T. and Fam, A. (2013), "Finite element analysis of beam-column T-joints of rectangular hollow steel sections strengthened using through-wall bolts", *Thin-Wall. Struct.*, **64**, 31-40.
- Yang, J., Shao, Y.B. and Chen, C. (2012), "Static strength of chord reinforced tubular Y-joints under axial loading", *Marine Struct.*, **29**(1), 226-245.

CC